Structure, Infrared and Raman spectroscopic studies of the new Ba(Nb$^V_{0.5}$$M^{III}_{0.5}$)(PO$_4$)$_2$ (M^{III} = Al, Cr, Fe, In) yavapaiite compounds 'series

Rachid Fakhreddine [*] **and Abderrahim Aatiq**

University Hassan II of Casablanca, Faculty of Sciences Ben M'Sik, Chemistry Department. Laboratory of Physical-Chemistry of Applied Materials, Avenue Idriss El Harti, B.P. 7955, Casablanca, Morocco

Abstract: Synthesis and structural study of the new Ba(Nb$^V_{0.50}$$M^{III}_{0.50}$)(PO$_4$)$_2$ (M^{III} = Al, Cr, Fe, In) phosphates, abbreviated as [BaNbM], were reported here for the first time. Structures of [BaNbM] compounds, obtained by solid-state reaction in air atmosphere, were determined at room temperature from X-ray powder diffraction using the Rietveld method. The four studied compounds feature the *yavapaiite*-type structure, with space group $C2/m$ (C^3_{2h}, N°12) and $Z = 2$. Their framework can be described as consisting of dense slabs of Nb(M)O$_6$ octahedra and PO$_4$ tetrahedra interconnected via corner-sharing, alternating along the c-axis with layers of Ba cations in ten-fold coordination. Raman and Infrared spectroscopic study were used to obtain further structural information about the nature of bonding in selected compositions. Assignments of Nb-O, M-O and P-O Raman and Infrared bands, in [BaNbM] compounds, were based on those already known in the literature for niobium and phosphates oxides. Some empirical relationships, connecting Raman stretching frequencies to the obtained Nb-O and P-O distance values, were also used for assignments of various Raman bands.

Keywords: Barium and Niobium phosphate; Yavapaiite structure; Raman and IR spectroscopy; Rietveld analysis.

Introduction

As a result of various cationic substitution in A sites of A^{III}PO$_4$ phases, a new family of oxides crystallising in several basic types as Monazite, Zircon (Xenotime), Scheelite, Cheralite, Nasicon and Yavapaiite compounds type have been synthesized and characterized [1-14]. Such materials can include a mixing of A^{II}/M^{IV} ions leading to the $A^{II}_{0.5}M^{IV}_{0.5}$PO$_4$ formula which was often reported as $A^{II}M^{IV}$(PO$_4$)$_2$ form (A = Ca, Sr, Ba, Pb; M = Ti, Ge, Zr, Mo, Sn, Th, U, Np, Pu) [3-8]. Practically all later compounds have been reported for their potential application as catalysts, ion exchangers, ionic conductors, immobilization of high-level nuclear waste materials and as luminescent materials [3,9-11]. For smaller M^{IV} ions, as in the BaM^{IV}(PO$_4$)$_2$ (M^{IV} = Ti, Ge, Zr, Mo, Sn, Hf) series, a monoclinic structure isotypic of the KFe(SO$_4$)$_2$ yavapaïte structure type ($C2/m$ space group, Z=2) is obtained [3-8]. Such structure-type can be described as made of layers of Ba^{II} cations in tenfold coordination, alternating with dense slabs built up of corner-connected of M^{IV}O$_6$ octahedra and PO$_4$ tetrahedra. Note that structure of $A^{II}M^{IV}$(PO$_4$)$_2$ phases is firmly dependent to the nature and/or size of the A^{II} and M^{IV} cations and many authors have attempted to establish a relationship between composition and crystal structure of some compounds [8].

Recently coupled substitution of M^{IV} cations by M'^{III}/M''^{V} ones within Nasicon A$^{II}_{0.5}M^{IV}_2$(PO$_4$)$_3$ and Yavapaiite A^{II}M^{IV}(PO$_4$)$_2$ type-phases were realized. Results of investigations led to synthesis and characterization of a series of $A^{II}_{0.5}$Sb^{V}Fe^{III}(PO$_4$)$_3$ (A = Mg, Ca, Mn, Ni, Sr, Cd, Pb) Nasicon phases ($P\bar{3}$ or $R\bar{3}$ space group) and new synthetic A^{II}(Sb$^V_{0.5}$Fe$^{III}_{0.5}$)(PO$_4$)$_2$ (A = Sr, Ba, Pb) Yavapaiite compounds [12-17].

Ba(Sb$^V_{0.5}$Fe$^{III}_{0.5}$)(PO$_4$)$_2$ features a true yavapaiite (TY) structure with space group $C2/m$ (Z=2) isotypic to KFe(SO$_4$)$_2$ [17]. Sr(Sb$^V_{0.5}$Fe$^{III}_{0.5}$)(PO$_4$)$_2$ and Pb(Sb$^V_{0.5}$Fe$^{III}_{0.5}$)(PO$_4$)$_2$ crystallize in the monoclinic system (space group $C2/c$, Z=4) with a distorted yavapaiite (DY) structure type [17]. Note that in all cases the [(Sb$_{0.5}$Fe$_{0.5}$)(PO$_4$)$_2$]$^{2-}$ yavapaiite framework appears well adapted to bigger Sr^{2+}, Pb^{2+} and Ba^{2+} cations while for smaller alkaline earth metal cations like Ca^{2+}, the [SbFe(PO$_4$)$_3$]$^-$ Nasicon framework seems to be the more stable [17]. So, in a continuation of our scientific search for new materials likely to exhibit interesting physical properties, synthesis and structural characterization of four new synthetic Ba(Nb$^V_{0.5}$$M^{III}_{0.5}$)(PO$_4$)$_2$ (M^{III} = Al, Cr, Fe, In) compounds are undertaken. Raman and Infrared spectroscopic studies were realized in order to obtain

further structural information about the nature of bonding in $Ba(Nb_{0.5}M_{0.5})(PO_4)_2$ (M^{III} = Al, Cr, Fe, In) compounds.

Experimental

Syntheses of the four $Ba(Nb^V_{0.5}M^{III}_{0.5})(PO_4)_2$ (M^{III} = Al, Cr, Fe, In) compounds, abbreviated as [BaNbM], were carried out using conventional solid-state reaction techniques. Powder crystalline samples were prepared from mixtures of M_2O_3 (M^{III} = Al, Cr, Fe, In) (Prolabo, 99 %), Nb_2O_5 (Riedel-de Haën, 99.9 %), $NH_4H_2PO_4$ (Riedel-de Haën, 99 %) and carbonate $BaCO_3$ (Riedel-de Haën, 99 %) in stoichiometric proportions. The mixtures were heated progressively with intermittent grinding at 200°C (12 h), 600°C (24 h), 750°C (24 h) and 800°C (48 h) in air. Additional treatments up to 850°C (48 h) are necessary for obtaining pure samples. Except for the color of the [BaNbCr] compound which is green, the other [BaNbM] (MIII = Al, Fe, In) materials are white.

The products of reactions were characterised by X-ray powder diffraction (XRPD) at room temperature with a Panalytical X′Pert-PRO (θ-2θ) diffractometer; (CuKα) radiation (45 kV, 40 mA). The data were collected over 8 h from 10 to 100° (2θ), in steps of 0.0167°. The Rietveld refinement of the structure was performed using the Fullprof program [18]. It was interesting to note that our attempt to synthesize "$CaNb_{0.50}M_{0.50}(PO_4)_2$" was not satisfactory, although identical synthesis conditions have been applied. Analysis of the obtained XRD spectra shows mainly the presence of a mixture of the already known $Ca_{0.50}NbM(PO_4)_3$ (M^{III} = Al, Fe, In) Nasicon phases [19] and other minority phosphate compounds.

The infrared spectra were recorded in the form of KBr pellets in the wave number range 1500-400 cm^{-1} using a Bruker's VERTEX 70 spectrometer, and the Raman spectra are recorded on RENISHAW 1000B spectrometer in the wave number range 400-1500 cm^{-1}. All the spectra have been recorded at room temperature.

Results and Discussion

According to the literature data, the obtained peak positions and intensities of the XRPD patterns of $Ba(Nb_{0.5}M_{0.5})(PO_4)_2$ (M^{III} = Al, Cr, Fe, In) are close to those of $Ba(Sb_{0.5}Fe_{0.5})(PO_4)_2$ ($C2/m$ space group, Z = 2) [17], therefore their XRPD patterns can be indexed, in a first approximation, on a similar monoclinic cell.

Rietveld refinement and structural description of $Ba(Nb_{0.5}M_{0.5})(PO_4)_2$ (M^{III} = Al, Cr, Fe, In) compounds
The Rietveld analysis in Le Bail's (profile matching) mode [20] confirmed that [BaNbM] phases are compatible with the $C2/m$ space group (C^3_{2h}, N°12).

So, initial starting parameters for the Rietveld refinement of $Ba(Nb_{0.5}M_{0.5})(PO_4)_2$ (M^{III} = Al, Cr, Fe, In) were based on those already reported for the true yavapaiite (*TY*) $Ba(Sb_{0.5}Fe_{0.5})(PO_4)_2$ phase in the $C2/m$ space group [17]. This refinement leads to acceptable reliability factors. Crystallographic data and reliability factors of the four [BaNbM] compounds are reported in Table 1. Results of the Rietveld refinement and selected interatomic distances are summarised in Tables 2 and 3 respectively. A comparison of the experimental and calculated XRPD profile of [BaNbM] (M^{III} = Al, Cr, Fe, In) materials is given in Figure 1.

Table 1. Crystallographic data of $Ba(Nb_{0.5}M_{0.5})(PO_4)_2$ (M= Al, Cr, Fe, In) ($C2/m$ space group, Z =2).

$Ba(Nb_{0.5}M_{0.5})(PO_4)_2$ (M=Al, Cr, Fe, In)	[BaNbAl]	[BaNbCr]	[BaNbFe]	[BaNbIn]
a(Å)	8.2955(1)	8.3103(4)	8.3462(4)	8.4095(1)
b(Å)	5.1654(2)	5.2069(3)	5.2289(1)	5.2746(3)
c(Å)	7.7344(1)	7.7579(4)	7.7770(4)	7.8761(4)
β(°)	93.890(1)	93.918(3)	93.934(1)	93.751(4)
V(Å³)	331(1)	335(3)	339(1)	348(2)
χ^2	1.39	1.58	1.36	1.44
R_P	0.061	0.080	0.062	0.056
R_{WP}	0.085	0.110	0.084	0.076
R_B	0.034	0.046	0.026	0.030
R_F	0.028	0.032	0.024	0.027

Table 2. Structural parameters of $Ba(Nb_{0.5}M_{0.5})(PO_4)_2$ (M= Al, Cr, Fe, In).

$Ba(Nb_{0.5}M_{0.5})(PO_4)_2$ (*M*=Al, Cr, Fe, In)	[BaNbAl]	[BaNbCr]	[BaNbFe]	[BaNbIn]
Ba 2c (0 0 0.5)				
B ($Å^2$)	1.6(1)	1.1(1)	2.0(1)	1.1(1)
Occupancy	1	1	1	1
Nb(M) 2a (0 0 0)				
B ($Å^2$)	1.5(1)	1.0(1)	1.5(1)	1.1(1)
Occupancy Nb/M	0.5/0.5	0.5/0.5	0.5/0.5	0.5/0.5
P 4i (x 0 z)				
x	0.3606(6)	0.3638(5)	0.3630(2)	0.3638(7)
z	0.2054(3)	0.2038(5)	0.2102(3)	0.2166(3)
B ($Å^2$)	1.6(2)	1.4(2)	1.6(5)	1.0(2)
Occupancy	1	1	1	1
O(1) 4i (x 0 z)				
x	0.2170(1)	0.2195(10)	0.2193(6)	0.2335(4)
z	0.0709(5)	0.0677(13)	0.0736(4)	0.0727(4)
B ($Å^2$)	1.2(5)	1.5(1)	1.3(1)	1.4(3)
Occupancy	1	1	1	1
O(2) 4i (x 0 z)				
x	0.3111(6)	0.3151(16)	0.3110(6)	0.3077(5)
z	0.3910(1)	0.3912(8)	0.3965(5)	0.3998(6)
B ($Å^2$)	1.7(1)	0.9(1)	1.3(1)	1.8(1)
Occupancy	1	1	1	1
O(3) 8j (x y z)				
x	0.4685(9)	0.4680(11)	0.4695(1)	0.4724(5)
y	0.2414(5)	0.2397(12)	0.2376(2)	0.2351(5)
z	0.1791(1)	0.1832(13)	0.1840(5)	0.1934(5)
B ($Å^2$)	1.8(1)	0.9(1)	1.3(1)	1.6(1)
Occupancy	1	1	1	1

Table 3. Selected interatomic distances (Å), calculated Bond Valence Sum (*BVS*) and octahedral Nb(*M*)O$_6$ distortion parameter (Δd) for $Ba(Nb_{0.5}M_{0.5})(PO_4)_2$ (*M*= Al, Cr, Fe, In). Nb(M)-*O** are the calculated distance from Shannon's table.

$Ba(Nb_{0.5}M_{0.5})(PO_4)_2$ (M=Al, Cr, Fe, In)	[BaNbAl]	[BaNbCr]	[BaNbFe]	[BaNbIn]
Nb(M)-O distances (Å)				
2×Nb(M)-O(1)	1.846(1)	1.863(5)	1.881(7)	2.009(5)
4×Nb(M)-O(3)	1.955(2)	1.995(3)	2.011(6)	2.091(3)
Aver.<Nb(M)-O>	1.92(1)	1.95(1)	1.97(1)	2.06(1)
Nb(M)-O*	1.99	2.03	2.04	2.12
BVS(Nb(M))	4.31	4.37	4.33	3.95
(should be)	(4)	(4)	(4)	(4)
(Δd×10^{-4})	7.16	10.18	58.10	21.25
P-O distances (Å)				
P-O(1)	1.528(2)	1.542(8)	1.544(5)	1.524(6)
P-O(2)	1.520(4)	1.536(7)	1.539(1)	1.547(1)
2×P-O(3)	1.556(1)	1.534(6)	1.551(3)	1.558(6)
Aver.<P-O>	1.54(1)	1.54(1)	1.55(1)	1.55(1)
BVS(P)	4.93	4.97	4.84	4.84
(should be)	(5)	(5)	(5)	(5)
Ba-O distances (Å)				
2×Ba-O(2)	2.770(1)	2.784(6)	2.790(6)	2.754(2)
4×Ba-O(3)	2.815(5)	2.799(4)	2.808(2)	2.786(1)
4×Ba-O(2)	3.107(3)	3.124(1)	3.129(3)	3.167(4)
Aver.<Ba-O>	2.92(1)	2.93(1)	2.93(1)	2.93(1)
BVS (Ba)	1.93	1.93	1.89	1.96
(should be)	(2)	(2)	(2)	(2)
Nb(M)-Nb(M) (Å)	4.89(1)	4.90(3)	4.92(4)	4.96(1)

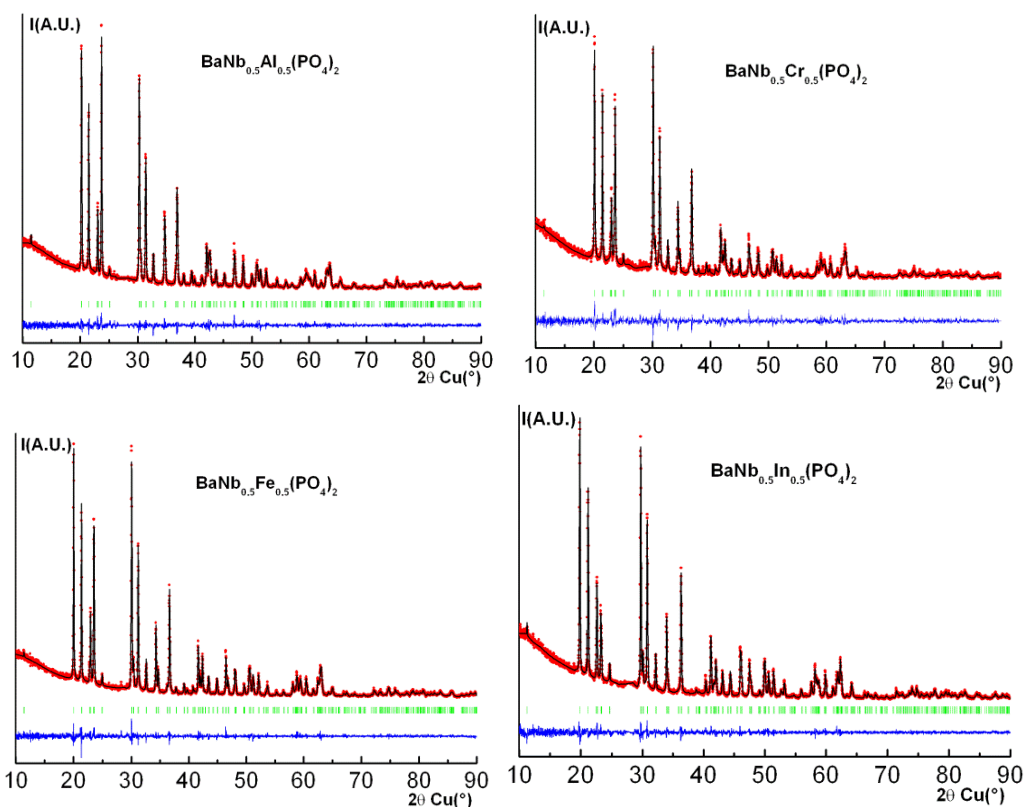**Figure 1.** Experimental (●●●) calculated (—), and difference profile (—) of the XRPD patterns of $Ba(Nb_{0.5}M_{0.5})(PO_4)_2$ (*M*=Al, Cr, Fe, In). Bars in green (|) indicate the Bragg peak positions

Structure of $Ba(Nb_{0.5}M_{0.5})(PO_4)_2$ compounds consists of three types of polyhedra, BaO_{10}, PO_4 and $Nb(M)O_6$ (Fig. 2). It can also be viewed as being composed of alternating edge-sharing BaO_{10} bicapped square antiprism and $Nb(M)O_6$ octahedra forming chains parallel to the c-axis (Fig. 2b). There are five chains per unit cell (Fig. 2a). Each $Nb(M)O_6$ octahedron is bound by its vertices to six PO_4 tetrahedra and shares two of its edges (i.e., O(3)-O(3) one) to two BaO_{10} polyhedra (Fig. 2). The framework can be described as consisting of dense slabs of $Nb(M)O_6$ octahedra and PO_4 tetrahedra interconnected via corner-sharing, alternating along the c-axis with layers of Ba cations in ten-fold coordination (Fig. 3). The ten oxygen atoms of each BaO_{10} polyhedron belong to six phosphate PO_4 groups (Fig. 2b). Eight of the oxygen atoms come from four bidentate PO_4 groups by sharing three O(2)-O(3) sides while the two other oxygens (i.e., O(2) ones) belong to the two other monodentate PO_4 groups (Fig. 2b). Projection in ab plane of the structure of [BaNb*M*] compounds shows that every BaO_{10} polyhedron is connected, via its O(2)-O(2) edges, to six neighbouring BaO_{10} polyhedra (Fig. 3c).
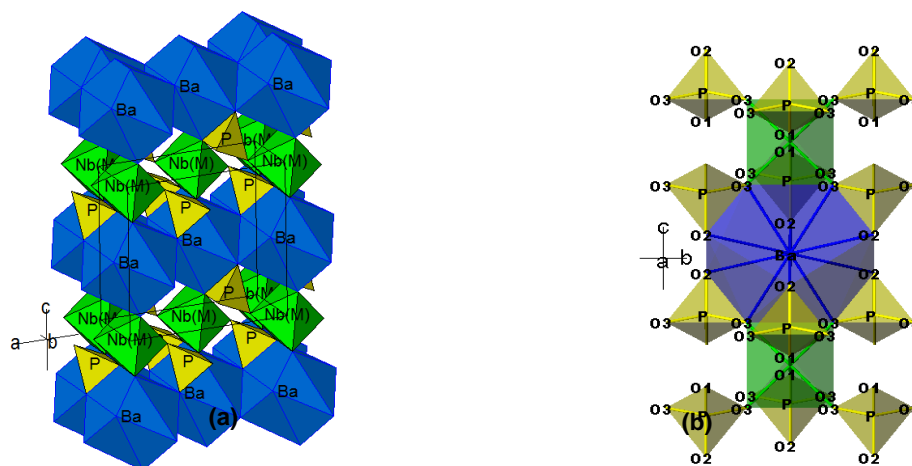

Figure 2. View of the structure in (a) and a row of BaO_{10}, PO_4 and $Nb(M)O_6$ polyhedra along c-axis in (b) of $Ba(Nb_{0.50}M_{0.50})(PO_4)_2$ (*M*=Al, Cr, Fe, In).
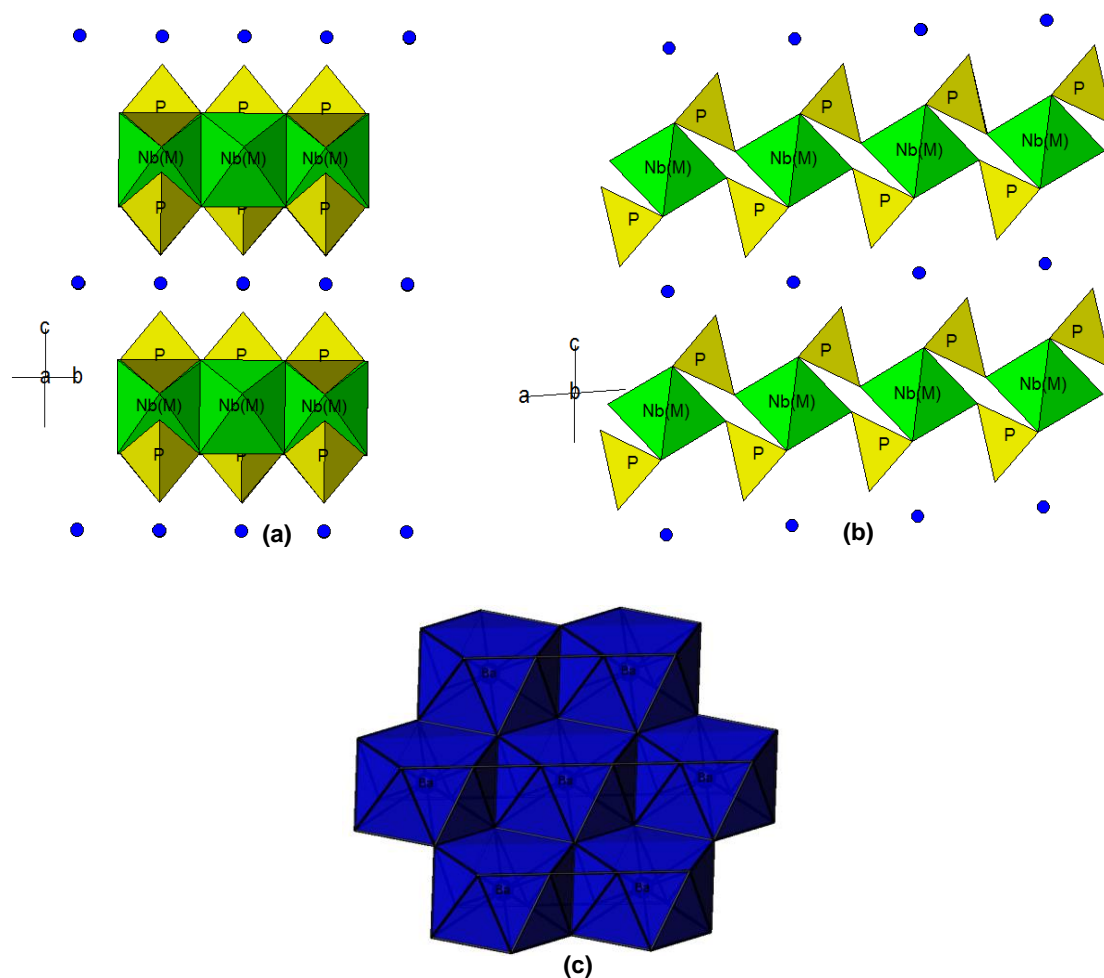
Figure 3. Projection in the *bc* plane (a), in the *ac* plane (b) and view of $BaO_{10}(BaO_{10})_6$ polyhedra (c) within the structure of $Ba(Nb_{0.50}M_{0.50})(PO_4)_2$ (*M*=Al, Cr, Fe, In). Barium atoms are represented by blue circles (●).

It is worthy to note that among the six Ba-Ba closest distances, the four shortest have a value of about 4.96(1) Å while the two the longest ones have a value around 5.27(1) Å. In fact, within each BaO_{10} polyhedron, the Ba-O distances values can divide into two groups (Table 3). The first group contains six relatively shortest Ba-O distances with values varying between 2.75 and 2.81 Å whereas the second group is formed by four longest Ba-O distances with an average value of 3.13 Å. Therefore, the coordinence of Ba atoms in [BaNb*M*] phases can be considered as 6+4. Ionic radii of Ba^{2+} in the tenfold coordination [$r(Ba^{2+}[X])$ =1.52 Å and $r(O^{2-}[VIII])$ = 1.42 Å] [21] predict the interatomic distances of 2.94 Å for Ba–O*. These last value is comparable with the mean $<Ba-O>=(2.93$ Å) interatomic distances obtained for [BaNb*M*] (*M*= Al, Cr, Fe, In) and $BaM(PO_4)_2$ (*M*= Ti, Sb(Fe), Mo, Zr) compounds [3,4,17,22] (Tables 2 and 4). P-O distances values match well with those typically observed in phosphates and the O-P-O angles vary between 105 and 116°. Obtained Nb(*M*)-O distances are consistent with the evolution of ionic radii values in six coordination of M^{3+} ions (*M* = Al, Cr, Fe, In) [21] (Table 3). Note that the calculated Nb(M)-O* distances values, from Shannon tables, are slightly higher by 0.07Å compared to those

experimentally obtained from the structural refinement (Table 3). A quantitative measure of the magnitude of the octahedral distortion parameter (Δd) is reported in Table 3. Analysis of the obtained *Δd* parameters shows that the octahedron $Nb(Fe)O_6$ is the most distorted. <Nb(M)-O> distances for [BaNbM] (*M*= Al, Cr, Fe, In) are relatively comparable to those already observed for the <M-O> distances in the $BaM(PO_4)_2$ (*M*= Ti, Sb(Fe), Mo, Zr) yavapaiite series [3,4,17,22] (Table 4). The gradual increase of *a*, *b*, *c* and V cells-parameters with the growing of M^{3+} crystal radius in [BaNb*M*] could be directly related to the progressive increase of Nb(*M*)-O and Nb(*M*)-Nb(*M*) interatomic distances (Fig. 4).

In order to have more structural information, the bond valence sum (*BVS*) based on bond strength analysis [23] for $Ba(Nb_{0.5}M_{0.5})(PO_4)_2$ were also computed. As shown in Table 3, the *BVS* values calculated for Ba, *M*, Nb and P sites are relatively consistent with the expected formal oxidation state of Ba^{2+}, M^{3+}, Nb^{5+} and P^{5+} ions. X-ray data, obtained from the ''observed intensities'' of the Rietveld refinement (CuKα1: 1.5406 Å), of [BaNb*M*] compounds, were given in Tables 5 and 6.

Table 4. Cell parameters, Ba-O and M-O distances for selected $BaM(PO_4)_2$ (*M*= Ti, Sb(Fe), Mo, Zr) yavapaiite compounds (*C2/m* space group, Z =2). *M-O** are the calculated distance from Shannon's table.

$BaM(PO_4)_2$	r_M^{4+}(Å)	a (Å)	b (Å)	c (Å)	β(°)	Ba-O (Å)	M-O (Å)
$BaTi(PO_4)_2$	0.605	8.273(3)	5.190(3)	7.737(3)	94.18(2)	2×Ba-O_2= 2.797(3) 4×Ba-O_3=2.813(2) 4×Ba-O_2=3.090(2 <Ba-O>=2.92(1)	2×Ti-O_1=1.878(3) 4×Ti-O_3=1.958(2) <Ti-O>=1.93(1) Ti-O*=2.00
$BaSb_{0.5}Fe_{0.5}(PO_4)_2$	$r_{<Sb(Fe)}$ = 0.62	8.156(8)	5.199(6)	7.829(1)	94.53(1)	2×Ba-O_2= 2.752(6) 4×Ba-O_3=2.829(4) 4×Ba-O_2=3.114(3) <Ba-O>=2.92(1)	2×M-O_1=1.895(5) 4×M-O_3=2.009(3) <Sb(Fe)-O>=1.95(1) Sb/Fe)-O*=2.02
$BaMo(PO_4)_2$	0.65	8.211(1)	5.276(3)	7.816(4)	94.77(8)	2×Ba-O_2= 2.790(5) 4×Ba-O_3=2.795(5) 4×Ba-O_2= 3.137(2) <Ba-O>=2.93(1)	2×Mo-O_1=1.947(7) 4×Mo-O_3=2.034(3) <Mo-O>=2.01(1) Mo-O*=2.05
$BaZr(PO_4)_2$	0.72	8.563(3)	5.308(2)	7.896(2)	93.09(1)	2×Ba-O_2= 2.835(7) 4×Ba-O_3=2.821(4) 4×Ba-O_2=3.162(3) Ba-O=2.96(1)	2×Zr-O_1=2.052(7) 4×Zr-O_3=2.073(4) <Zr-O>=2.07(1) Zr-O*=2.12
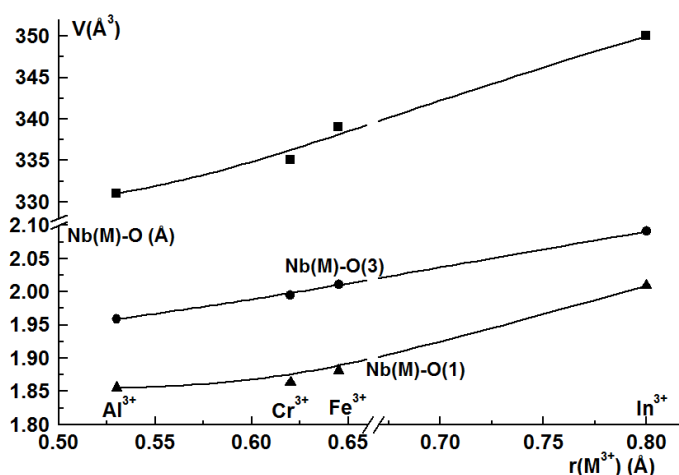
Figure 4. Evolutions of the cell-volume V (in $Å^3$) and the Nb(*M*)-O interatomic distances (in Å), with the M^{3+} crystal radii values (in Å) in six coordination for $Ba(Nb_{0.5}M_{0.5})(PO_4)_2$ (*M^{III}* = Al, Cr, Fe, In)

Raman and IR spectroscopy

In order to characterize further the $Ba(Nb_{0.5}M_{0.5})(PO_4)_2$ (*M^{III}* = Al, Fe, In) series of compounds, we have recorded and analyzed their Raman and infrared spectra (Fig. 5a and 5b) with their structural peculiarities. Given that the [BaNb*M*] yavapaiite structure can be described as consisting of dense slabs of Nb(M)O_6 octahedra and PO_4 tetrahedra interconnected via corner-sharing, alternating along the c-axis with layers of Ba cations in ten-fold coordination, such frameworks can be considered as formed by isolated PO_4 groups and isolated Nb(*M*)O_6 groups. Therefore, the vibrational spectrum is typical of orthophosphate. The crystal structure refinement shows that M^{3+} ions (*M* = Al, Fe, In) are occupying the Nb equivalents 'sites. Hence the NbO$_6$ octahedra will be probably disturbed by the presence of M^{3+} ions

in the equivalent site. It should be noticed that except the Fe^{3+} (HS) crystal radius (r_{Fe}^{3+} = 0.645 Å) in the octahedral environment, which is comparable to that of Nb^{5+} (r_{Nb}^{5+} = 0.64 Å) one, values of crystal radii size of the two other M^{3+} cations (i.e., Al^{3+} (r_{Al}^{3+} = 0.53 Å) and In^{3+} (r_{In}^{3+} = 0.80 Å)) show a notable difference with that of Nb^{5+} [21]. Given that structural data shows different types of Nb/*M*-O bonds in [BaNb*M*] phases, there will be a higher probability of M^{3+} ions disturbing Nb-O-P chain. This phenomenon will undoubtedly complicate assignments of different vibrations modes. Also, the coupling between PO_4 and NbO_6 modes as well as between NbO_6 and *M*O_6 vibrations in [BaNb*M*] should be expected. In all cases, assignments of the Raman and IR Nb–O, *M*–O and P–O bands were based on the already known niobium and phosphates oxide structures [24-28].

Table 5. Powder diffraction data of the two $Ba(Nb_{0.5}M_{0.5})(PO_4)_2$ (M= Al, Cr) compounds. Diffraction lines with I_{obs}< 1 are omitted ($CuK\alpha_1$; λ = 1.5406 Å).

Ba(Nb0.5Al0.5)(PO4)2				Ba(Nb0.5Cr0.5)(PO4)2			
hkl	d_{obs} (Å)	100 I/I_0 (obs.)	100 I/I_0 (cal.)	*hkl*	d_{obs} (Å)	100 I/I_0 (obs.)	100 I/I_0 (cal.)
001	7.7166	3	1	001	7.7398	3	2
110	4.3820	91	90	110	4.4095	100	98
200	4.1382	64	65	200	4.1455	80	78
-111	3.8706	4	3	-111	3.8926	6	5
002	3.8583	28	25	002	3.8699	34	32
-201	3.7545	100	99	111	3.7728	76	74
111	3.7530	65	65	-201	3.7629	30	30
201	3.5480	7	5	201	3.5546	7	5
-112	2.9488	81	80	-112	2.9625	97	98
-202	2.9226	11	11	-202	2.9305	12	12
112	2.8455	51	50	112	2.8576	64	62
202	2.7311	15	15	202	2.7371	15	17
020	2.5827	33	34	020	2.6035	39	41
003	2.5722	13	12	003	2.5799	11	10
021	2.4492	6	5	021	2.4676	4	3
310	2.4335	40	38	310	2.4411	47	48
-311	2.3620	6	6	-311	2.3694	4	4
311	2.2820	8	7	311	2.2888	7	7
-203	2.2542	4	3	-203	2.2608	4	3
220	2.1910	2	3	220	2.2047	6	5
113	2.1843	2	2	022	2.1601	24	24
022	2.1462	16	16	-221	2.1410	13	12
-221	2.1279	13	12	203	2.1262	7	7
203	2.1210	9	9	-312	2.1233	16	16
-312	2.1162	14	14	400	2.0727	13	13
221	2.0881	2	2	312	2.0106	13	12
400	2.0691	10	11	-222	1.9463	22	20
-401	2.0333	1	1	004	1.9349	8	8
312	2.0048	9	9	222	1.8864	16	14
-222	1.9353	17	13	-402	1.8814	6	6
004	1.9291	7	7	-313	1.8291	8	7
-402	1.8773	5	5	-204	1.8012	17	16
222	1.8765	14	13	-114	1.7960	11	12
-313	1.8230	8	8	402	1.7773	16	16
-204	1.7958	16	15	114	1.7486	16	14
-114	1.7895	8	7	204	1.7092	2	2
402	1.7740	13	14	130	1.6988	8	8
114	1.7427	13	13	131	1.6545	2	2
204	1.7047	2	2	420	1.6216	5	4
130	1.6857	6	6	510	1.5800	13	12
131	1.6422	4	4	-132	1.5636	15	14
420	1.6148	3	3	-314	1.5630	5	4
510	1.5763	9	9	024	1.5530	9	8
-314	1.5578	5	6	132	1.5476	10	8
-132	1.5526	11	11	-422	1.5249	17	16
024	1.5456	9	8	-512	1.4973	8	8
132	1.5369	13	10	-224	1.4812	16	14
-422	1.5185	13	14	-115	1.4774	1	1
-512	1.4934	5	5	314	1.4737	12	12
-224	1.4744	13	12	330	1.4698	13	13
314	1.4693	10	10	422	1.4679	18	16
422	1.4623	12	12	-404	1.4652	2	2

Table 6. Powder diffraction data of the two $Ba(Nb_{0.5}M_{0.5})(PO_4)_2$ ($M=$ Fe, In) compounds. Diffraction lines with $I_{obs} < 1$ are omitted ($CuK\alpha_1$; $\lambda = 1.5406$ Å).

Ba(Nb₀.₅Fe₀.₅)(PO₄)₂				Ba(Nb₀.₅In₀.₅)(PO₄)₂			
hkl	d_{obs} (Å)	100 I/I_0 (obs.)	100 I/I_0 (cal.)	*hkl*	d_{obs} (Å)	100 I/I_0 (obs.)	100 I/I_0 (cal.)
001	7.7586	3	3	001	7.8593	2	4
110	4.4281	97	95	110	4.4657	100	100
200	4.1632	70	73	200	4.1957	70	71
-111	3.9077	9	7	-111	3.9421	16	15
002	3.8793	32	29	002	3.9296	40	37
111	3.7868	61	61	111	3.8259	15	14
-201	3.7781	69	66	-201	3.8062	20	19
201	3.5679	5	5	201	3.6046	6	7
-112	2.9722	100	99	-112	3.0024	98	96
-202	2.9406	14	13	-202	2.9666	13	13
112	2.8666	62	61	112	2.9004	69	67
202	2.7457	10	13	202	2.7789	14	14
020	2.6144	30	27	020	2.6373	18	17
003	2.5862	11	10	003	2.6197	6	6
021	2.4776	4	3	021	2.5003	1	1
310	2.4516	46	44	310	2.4712	50	48
-311	2.3794	3	2	-311	2.3974	1	1
311	2.2980	3	4	311	2.3193	3	2
-203	2.2677	2	2	-113	2.2948	7	6
220	2.2141	3	3	220	2.2328	3	3
022	2.1680	22	19	022	2.1898	24	23
-221	2.1499	7	5	-221	2.1678	5	5
203	2.1323	5	5	203	2.1596	5	5
-312	2.1316	14	13	-312	2.1486	14	14
400	2.0816	7	7	400	2.0979	10	9
312	2.0179	7	7	312	2.0395	8	9
-222	1.9539	19	16	-222	1.9710	19	18
004	1.9397	7	6	004	1.9648	15	15
222	1.8934	10	10	222	1.9129	15	13
-402	1.8890	4	4	-402	1.9031	6	7
-313	1.8356	5	5	-313	1.8518	2	2
-204	1.8063	11	11	-204	1.8258	12	13
-114	1.8010	6	6	-114	1.8220	16	14
402	1.7840	8	9	402	1.8023	8	8
114	1.7533	9	9	114	1.7758	10	10
204	1.7138	2	2	204	1.7363	2	3
130	1.7060	6	5	130	1.7208	6	5
131	1.6613	3	2	131	1.6763	2	2
420	1.6285	3	2	420	1.6418	3	3
510	1.5868	6	5	510	1.5993	5	6
-132	1.5698	11	9	-132	1.5841	11	10
-314	1.5681	8	7	-314	1.5831	9	10
024	1.5578	9	8	024	1.5756	6	6
132	1.5536	8	7	132	1.5686	6	6
-422	1.5312	9	8	-422	1.5433	10	9
-512	1.5035	3	3	-512	1.5146	4	4
-224	1.4861	8	7	-224	1.5012	9	7
314	1.4782	13	11	314	1.4964	9	9
330	1.4761	13	11	330	1.4886	10	10
422	1.4736	7	8	422	1.4880	10	9
-404	1.4703	3	3	-404	1.4833	7	6
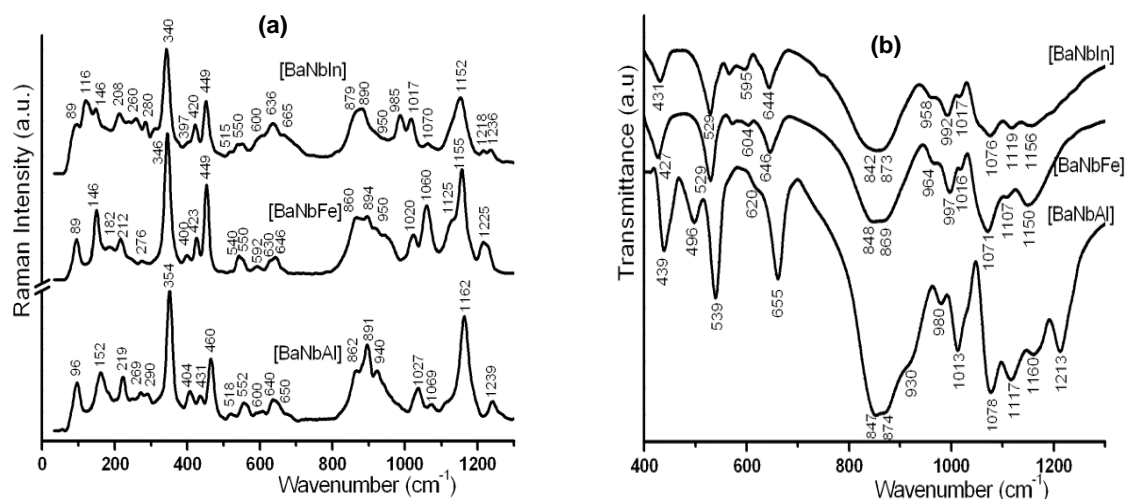
Figure 5. Raman spectra in (a) and IR spectra in (b) of $Ba(Nb_{0.5}M_{0.5})(PO_4)_2$ (M=Al, Fe, In).

Theory

As the Raman and IR spectra of $Ba(Nb_{0.50}M_{0.50})(PO_4)_2$ (Fig. 5) are essentially dominated by the internal vibrations of the PO_4 groups, and in order to facilitate assignments of different vibrations modes; we have performed a factor group analysis by correlating the internal vibrations modes of PO_4 groups between its point group (T_d), symmetry of the free ion, its site-group (C_s) and its factor group (C_{2h}) (Table 7). Analyses show that the four $v_1(A_1)$, $v_2(E)$, v_3 (F_2) and v_4 (F_2) PO_4 modes are Raman and IR active. As it will be shown later, band positions of the four PO_4 modes observed in the [BaNbM] spectra are close to those expected for yavapaiite phosphate-type materials [24].

In metal-oxide systems containing niobium, the binding forces within the metal-oxygen octahedra are higher than the crystal binding forces. External modes usually appear at lower frequencies than internal modes [25]. The free XO_6 octahedra ion with O_h symmetry has six fundamental modes of vibration, viz, symmetric stretching mode v_1 (A_{1g}), asymmetric stretching modes v_2 (E_g) and v_3 (F_{1u}), asymmetric bending mode v_4 (F_{1u}), symmetric bending mode v_5 (F_{2g}) and the Raman and IR inactive mode v_6 (F_{2u}). The factor group analysis for the internal vibrations [29], correlating the point group of the 'free' ion (O_h) with its site-group (C_{2h}) and its factor group (C_{2h}) is given in Table 8. The v_1, v_2 and v_5 modes are Raman active while v_3 and v_4 are IR active [30]. In most cases, the order of stretching frequencies is $v_{1 > v_3 >> v_2}$ whereas that of the bending one frequencies is $v_{4> v_{5>>} v_6}$ [30]. Note that the Nb^{5+} ion is too small to form regular octahedra in most of the oxide systems, and therefore it loses its O_h symmetry depending on the extent of distortion. Usually the distorted XO_6 octahedra can have any of the five symmetries, viz D_{4h}, D_{3d}, C_{4v}, C_{3v} or C_{2v} [25] but in the case of the $Ba(Nb_{0.5}M_{0.5})(PO_4)_2$ (M = Al, Fe, In) compounds, the site symmetry of distorted XO_6 is exactly C_{2h} (Table 7).

Table 7. Factor group analysis of the internal vibrations of the $(PO_4)^{3-}$ in $Ba(Nb_{0.5}M_{0.5})(PO_4)_2$ (M = Al, Fe, In) (space group $C2/m$).

vibration	Point group (T_d)	Site group (C_s)	Factor group (C_{2h})
v_1	A_1	A'	A_g+B_u
v_2	E	A'+A''	$A_g+B_u+A_u+B_g$
v_3	F_2	2A'+A''	$2A_g+2B_u+A_u+B_g$
v_4	F_2	2A'+A''	$2A_g+2B_u+A_u+B_g$
Activity Point group: A_1, E, F_2 (R); F_2 (IR) Site group: A, A'' (R, IR) Factor group: Ag, Bg (R); Au, Bu (IR)			

Table 8. Factor group analysis of the internal vibrations of the XO_6 ($X =M$(Nb) in Ba(Nb$_{0.5}$$M_{0.5}$)(PO$_4$)$_2$ (M = Al, Fe, In) (space group $C2/m$).

vibration	Point group (O$_h$)	Site group (C$_{2h}$)	Factor group (C$_{2h}$)
ν_1	A$_{1g}$	A$_g$	A$_g$
ν_2	E$_g$	2 A$_g$	2 A$_g$
ν_3	F$_{1u}$	A$_u$ + 2 B$_u$	A$_u$ + 2 B$_u$
ν_4	F$_{1u}$	A$_u$ + 2 B$_u$	A$_u$ + 2 B$_u$
ν_5	F$_{2g}$	A$_g$ + 2 B$_g$	A$_g$ + 2 B$_g$
ν_6	F$_{2u}$	A$_u$ + 2 B$_u$	A$_u$ + 2 B$_u$

Activity
Point group: A$_{1g}$, E$_g$, F$_{2g}$ (R); F$_{1u}$ (IR); F$_{2u}$ (In)
Site group: A$_g$, B$_g$ (R); A$_u$, B$_u$ (IR)
Factor group: Ag, Bg (R); Au, Bu (IR)

Vibrations of PO$_4^{3-}$ tetrahedral

Proposed assignments of IR and Raman bands corresponding to PO$_4^{3-}$ groups are given in Table 9. Thus, the symmetric non degenerate P-O stretching modes ($\nu_{1(P-O)}$) are observed in the Raman and IR spectra around 950 cm^{-1} while the three predicted modes corresponding to the antisymmetric and doubly degenerate PO stretching ($\nu_{3(P-O)}$) are attributed to the three Raman and IR bands observed in the vicinity of 990, 1020 and 1070 cm^{-1}. The two bands obtained around 420 and 450 cm^{-1} are attributed to the symmetric, triply degenerate O-P-O bending ($\nu_{2(OPO)}$) modes. As will be seen in the following, the $\nu_{2(OPO)}$ bands are coupled with the $\nu_{4(Nb-O)}$ stretching modes of NbO$_6$ octahedra. Three predicted Raman and IR bands of antisymmetric and harmonic O-P-O bending ($\nu_{4(OPO)}$) are observed around 520, 600 and 660 cm^{-1}. The $\nu_{4(OPO)}$ bands are also coupled with the only Raman active $\nu_{2(Nb-O)}$ stretching bands of NbO$_6$ octahedra (Table 9). It should be noticed that in [BaNbM], P–O distances vary between 1.515(1) and 1.558(1) Å with a mean P–O distance of 1.54 Å. Popovic et al. have formulated the following empirical relation [$\nu_{(P-O)}$ (cm^{-1}) = 224500 exp(-R/28.35)] which connects P–O bond lengths and stretching frequencies where R is the P–O bond lengths in Picometer (pm) [28]. By replacing P-O distance values in the above expression, the calculated frequencies values are respectively 1072 cm^{-1}, 982 cm^{-1} and 922 cm^{-1}. These last values are much well with those experimentally observed, between 930 and 1050 cm^{-1} in the Raman spectra of [BaNbM], for the two $\nu_{1(P-O)}$ and $\nu_{3(P-O)}$ stretching modes of PO$_4$ tetrahedra (Table 9).

Vibrations of Nb(M)O$_6$ octahedra

The Nb-O…P bonds existing in [BaNbM] compounds have a length varying between 1.85 and 2.09 Å. In crystals containing NbO$_6$ octahedra, Hardcastle and Wachs have formulated an empirical relation [$\nu_{(Nb-O)}$ (cm^{-1}) = 25 922 exp(-1.9168 R)], connecting the Nb–O bond lengths and Raman scattering frequencies where R is the Nb–O bond length in ångström (Å)[27]. Substitution of the obtained Nb–O bond length in the NbO$_6$ octahedra gives $\nu_{(Nb-O)}$ Raman frequencies values between 470 and 750 cm^{-1}. Note that the $\nu_{2(Nb-O)}$ stretching vibrations, which are attributed to the observed bands around 550 and 640 cm^{-1}, are in agreement with Hardcastle's relation. It should be noticed that stretching Nb–O modes are usually observed between 550 and 890 cm^{-1}. Given that $\nu_{3(Nb-O)}$ stretching vibrations are only IR active mode, bands observed at around 850 and 890 cm^{-1} in the IR spectra of [BaNbM] could be attributed to the stretching $\nu_{3(Nb-O)}$ vibrations. The other Raman bands observed around 870 cm^{-1} are attributed to the $\nu_{1(Nb-O)}$ stretching modes. In Na$_4$Nb(PO$_4$)$_3$ the high Nb–O intensity band is observed at 900 cm^{-1} [26]. It is important to emphasize that the presence of more than one predicted Raman bands (Table 9), could be explained by the fact that in the case where more than one type of XO_6 octahedron are present, as it is in the [BaNbM] phases; multiple Raman bands due to $\nu_{(Nb-O)}$ and $\nu_{(M-O)}$ of Nb(M)O$_6$ (M=Al, Fe, In) octahedra should be seen [25]. The band observed in the IR spectra at around 430 cm^{-1} and which is coupled with the bending $\nu_{2(OPO)}$ modes could be attributed to the $\nu_{4(ONbO)}$ bending modes. In the 420-460 cm^{-1} frequency range, strong coupling between different O-P-O, O-Nb-O and Nb-O-P bending vibrations have been observed. The other Raman bands observed at 350 cm^{-1} and 400 cm^{-1} could be assigned to the $\nu_{5(ONbO)}$ and ν_{M-O} (M=Al, Fe, In) bands. Similar Raman bands, already observed at 364 and 370 cm^{-1}, were also attributed to Fe^{3+}-O stretching modes in $M_{0.5}$SbFe(PO$_4$)$_3$ (M = Mg, Ca, Ni, Sr, Pb) [12,15,16] and Li$_3$Fe$_2$(PO$_4$)$_3$ phases [34]. For [BaNbM] materials, the position of the $\nu_{6(ONbO)}$ band should be predicted to be shown between 260 and 280 cm^{-1} within the region of the external mode. In low-frequency modes and more precisely for values below 270 cm^{-1}, the translational modes of Ba^{2+}, M^{3+}, Nb^{5+} and PO$_4^{3-}$ ions as well as vibrational modes of PO$_4^{3-}$ ions MO$_6$, and NbO$_6$ groups should be expected.

Table 9. Spectral data (cm^{-1}) and proposed IR and Raman band assignments for Ba(Nb$_{0.5}$$M_{0.5}$)(PO$_4$)$_2$ (M = Al, Fe, In).

[BaNbAl]		[BaNbFe]		[BaNbIn]		Assignments
IR	Raman	IR	Raman	IR	Raman	
	96		89		89	External modes
	152		146		116	
			182		146	
	219		212		208	
	269				260	ν_6(Nb-O)
	290		276		280	
	354		346		340	ν_5(Nb-O) +
	404		400		397	ν(M-O)
	431		423		420	ν_2(PO$_4$)
439		427		431		+
496	460		449		449	ν_4(Nb-O)
539	518	529	540	529	515	
	552		550		550	ν_4(PO$_4$)
	600	604	592	595	600	+
620	640		630		636	ν_2(Nb-O)
655	650	646	646	644	665	
847		848		842		ν_3(Nb-O)
874		869		873		
	862		860		879	ν_1(Nb-O) + ν(M-O)
	891		894		890	
930	940	964	950	958	950	ν_1(PO$_4$)
980		997		992	985	
1013	1027	1016	1020	1017	1017	ν_3(PO$_4$)
1078	1069	1071	1060	1076	1070	
1117		1107	1125	1119	1152	ν(PO$_4$) /ν(M-O)
1160	1162	1150	1155	1156		interaction
1213			1225	1205	1218	
	1239				1236	

Conclusion

A series of new Ba(Nb$^{V}_{0.5}$$M^{III}_{0.5}$)(PO$_4$)$_2$ (M^{III} = Al, Cr, Fe, In) double phosphate were prepared by solid-state reaction method and structurally characterized from X-ray powder diffraction using the Rietveld method and by Raman and infrared spectroscopy. The four [BaNbM] materials feature the yavapaiite-type structure, with space group $C2/m$. The [(Nb$_{0.5}$$M_{0.5}$)(PO$_4$)$_2$]$^{2-}$ yavapaiite framework appears well adapted to bigger Ba^{2+} cations. In contrast to this, in the case of small alkaline earth metal cations, the Nasicon framework seems to be the more stable. By applying our experiment conditions, the use of large cations such as Sr^{2+} or Pb^{2+} shows an important competition between the corresponding yavaipaiite type-phase and other secondary phases. Observed Raman and IR bands are assigned in terms of vibrations of Nb(M)O$_6$ octahedra and PO$_4$ tetrahedra. Researches on potential application of [BaNbM] phases are in progress.

References

1- N. Clavier, R. Podor, N. Dacheux, Crystal chemistry of the monazite structure, J. Eur. Ceram. Soc., **2011**, 31, 941-976.

2- J. J. Finney, N. Nagaraja Rao, The crystal structure of Chéralite, Am. Mineral., **1967**, 52, 13-19.

3- K. Fukuda, A. Moriyama, T. Iwata, Crystal structure, phase transition and anisotropic thermal expansion of barium zirconium diorthophosphate, BaZr(PO$_4$)$_2$, J. Solid State Chem., **2005**, 178, 2144-2151.

4- A. Leclaire, M. M. Barel, J. Chardon, B. Raveau, A Mo(IV) Monophosphate, BaMo(PO$_4$)$_2$, with the Yavapaiite Layer Structure, J. Solid State Chem., **1995**, 116, 364-368.

5- K. Popa, G. Wallez, D. Bregiroux, P. Loiseau, M^{II}Ge(PO$_4$)$_2$ (M=Ca, Sr, Ba) Crystal structure, phase transitions and thermal expansion, J. Solid State Chem., **2011**, 184, 2629-2634.

6- D. Zhao, H. Zhang, Z. Xie, W. L. Zhang, S. L. Yang, W. D. Cheng, Syntheses, crystal and electronic structures of compounds AM(PO$_4$)$_2$ (A = Sr, M = Ti, Sn; A = Ba, M = Sn), Dalton Trans., **2009**, 27, 5310-5318.

7- W. L. Zhang, C. S. Lin, Z. Z. He, H. Zhang,

Z. Z. Luo, W. D. Cheng, Syntheses of three members of $A^{(II)}M^{(IV)}(PO_4)_2$: luminescence properties of $PbGe(PO_4)_2$ and its Eu^{3+} doped powders, Cryst. Eng. Comm., **2013**, 15, 7089-7094.

8- G. Wallez, D. Bregiroux, K. Popa, P. E. Raison, C. Apostolidis, P. Lindqvist-Reis, R. J. M. Konings, A. F. Popa, $BaAn^{IV}(PO_4)_2$ (An^{IV} = Th, Np) A New Family of Layered Double Phosphates, J. Inorg. Chem., **2011**, 110-115.

9- E. Morin, G. Wallez, S. Jaulmes, J. C. Couturier, M. Quarton, Structure of $Pb^{II}Sn^{IV}(PO_4)_2$: Stereochemical Activity of the Lead II Lone Pair, J. Solid State Chem., **1998**, 137, 283-288.

10- G. Blasse, G. J. Dirksen, The luminescence of Barium Titanium Phosphate $BaTi(PO_4)_2$, Chem. Phys. Lett., **1979**, 62, 19-20.

11- Z. J. Zhang, J. L. Yuan, X. J. Wang, D. B. Xiong, H. H. Chen, J. T. Zhao, Y. B. Fu, Z. M. Qi, G. B. Zhang, C. S. Shi, Luminescence properties of $CaZr(PO_4)_2$: RE (RE = Eu^{3+}, Tb^{3+}, Tm^{3+}) under x-ray and VUV–UV excitation, Phys. D Appl. Phys., **2007**, 40, 1910-1914.

12- A. Aatiq, R. Hassine, R. Tigha, I. Saadoune, Structures of two newly synthesized $A_{0.50}SbFe(PO_4)_3$ (A=Mn, Cd) Nasicon phases, Powder Diffr., **2005**, 20, 33-39.

13- A. Aatiq, R. Tigha, S. Benmokhtar, Structure, infrared and Raman spectroscopic studies of new $Sr_{0.50}SbFe$ $(PO_4)_3$ and $SrSb_{0.50}Fe_{1.50}$ $(PO_4)_3$ Nasicon phases, J. Mater. Sci., **2012**, 47, 1354-1364.

14- A. Aatiq, R. Tigha, R. Hassine, I. Saadoune, Crystallochemistry and structural studies of two newly $CaSb_{0.50}Fe_{1.50}(PO_4)_3$ and $Ca_{0.50}SbFe(PO_4)_3$ Nasicon phases, Powder Diffr., **2006**, 21, 45-51.

15- A. Aatiq, My R. Tigha, R. Fakhreddine, A. Marchoud, Structure and spectroscopic characterization of the two $PbSb_{0.5}Fe_{1.5}(PO_4)_3$ and $Pb_{0.5}SbFe(PO_4)_3$ phosphates with Nasicon type-structure, J. Mater. Environ. Sci., **2015**, 6, 3483-3490.

16- A. Aatiq, A. Marchoud, H. Bellefquih, My R. Tigha, Structural and Raman spectroscopic studies of the two $M_{0.50}SbFe(PO_4)_3$ (M = Mg, Ni) NASICON phases Powder Diffr., **2017**, 32, 40-51.

17- A. Aatiq, My R. Tigha, R. Fakhreddine, D. Bregiroux, G. Wallez, Structure, infrared and Raman spectroscopic studies of newly synthetic $A^{II}(Sb^{V}_{0.50}Fe^{III}_{0.50})(PO_4)_2$ (A=Ba, Sr, Pb) phosphates with yavapaiite structure Solid State Sci., **2016**, 58, 44-54.

18- J. Rodríguez-Carvajal, Recent advances in magnetic structure determination by neutron powder diffraction Physica B. Condensed Matter., **1993**, 192, 55-69.

19- B. Srinivasulu, M. Vithal, Preparation of a new family of NASICON type phosphates $Ca_{0.5}NbMP_3O_{12}$ (M = Fe, Al, Ga and In) and characterization of the iron systems by Mossbauer spectroscopy Mater. Sci. Lett., **1999**, 18, 1771-1773.

20- A. Le Bail, H. Duroy, J. L. Fourquet, Ab-initio structure determination of $LiSbWO_6$ by X-ray powder diffraction, Mater. Res. Bull., **1988**, 23, 447-452.

21- R. D. Shannon, Revised effective ionic radii and systematic studies of interatomic distances in halides and chalcogenides Acta Crystallographica Section A, **1988**, 32, 751-767.

22- D. Zhao, Fa-X. Ma, H. Yang, W. Wei, Y.-C. Fan, L. Zhang, X. Xin, Structure twinning, electronic and photoluminescence properties of yavapaiite-type orthophosphate $BaTi(PO_4)_2$, J. Phys. Chem. Solids, **2016**, 99, 59–65

23- I. D. Brown, D. Altermatt, Bond-valence parameters obtained from a systematic analysis of the Inorganic Crystal Structure Database Acta Cryst. Section B, **1985**, 41, 244-247.

24- M. Th. Paques-Ledent, $A^{II}B^{IV}(XO_4)_2$ Phosphates and Arsenates with Yavapaiite structure I: isostructural relationship and vibrational study, Inorg. Nucl. Chem., **1977**, 39, 11-17.

25- A. Ann McConnel, J. S. Aderson, C. N. R. Rao, Raman spectra of niobium oxides, A Mol. Biomol. Spectrosc., **1976**, 32, 1067-1076.

26- A. El Jazouli, C. Parent, J. M. Dance, G. Le Flem, P. Hagenmuller, J. C. Viala, $Na_4Nb(PO_4)_3$, a material with a reversible crystal-glass transformation: Structural and optical comparison, J. Solid State Chem., **1988**, 74, 377-384.

27- F. D. Hardcastle, I. E. Wachs, Determination of niobium-oxygen bond distances and bond orders by Raman spectroscopy, Solid State Ion., **1991**, 45, 201-213.

28- L. Popović, D. de Waal, J. C. A. Boeyens, Correlation between Raman wavenumbers and P—O bond lengths in crystalline inorganic phosphates, J. Raman Spectrosc., **2005**, 36, 2-11.

29- W. G. Fateley, F. R. Dollish, N. T. McDevitt, F.F. Bentley, Infrared and Raman selection rules for molecular and lattice vibrations the correlation method, Wiley-Interscience, New York, **1972**.

30- K. Nakamoto, Infrared and Raman Spectra of Inorganic and Coordination Compounds, Part A, Fifth ed, Wiley–Interscience, New York **1997**.

31- G. Butt, N. Sammes, G. Tompsett, A. Smirnova, O. Yamamoto, Raman spectroscopy of superionic Ti-doped $Li_3Fe_2(PO_4)_3$ and $LiNiPO_4$ structures, J. Power sources, **2004**, 134, 72-79.